Earth and Planetary Science Letters 299 (2010) 1–9

Contents lists available at ScienceDirect

Earth and Planetary Science Letters

journal homepage: www.elsevier.com/locate/epsl

Tracking deep mantle reservoirs with ultra-low velocity zones

Allen K. McNamara [a,*], Edward J. Garnero [a], Sebastian Rost [b]

[a] Arizona State University, School of Earth and Space Exploration, PO Box 871404, Tempe, AZ 85287-1404
[b] University of Leeds, School of Earth and Environment, Leeds, LS2 9JT United Kingdom

ARTICLE INFO

Article history:
Received 8 April 2010
Received in revised form 23 July 2010
Accepted 23 July 2010
Available online 28 September 2010

Editor: Y. Ricard

Keywords:
ULVZ
mantle convection
LLVSPs
core–mantle boundary

ABSTRACT

Some regions of the Earth's lowermost mantle exhibit anomalous seismic properties within a thin zone, less than tens of kilometers in thickness, that directly overlies the core-mantle boundary (CMB). These regions have been dubbed Ultra-Low Velocity Zones (ULVZs) due to their greater than 10% drop in seismic velocities. High resolution seismic array studies have found small, localized ULVZs (e.g., 10 km thick and 50-100 km wide) with a large increase in ULVZ density (~10%) relative to the background mantle. Many studies note that ULVZ material may be chemically distinct, though P-to-S-wave velocity reductions are sometimes consistent with partial melting. The apparent absence of ULVZs in many regions of the CMB is consistent with having a distinct chemical signature, regardless of melt content. However, it is unknown how a small volume of very dense ULVZ material can be locally elevated, particularly in the presence of large-scale compositional reservoirs predicted by seismology, geochemistry, and geodynamics. We perform ultra-high resolution, kilometer-scale, thermochemical convection calculations for an entire mantle system containing three distinct compositional components in order to investigate how a ULVZ interacts with large-scale lower mantle compositional reservoirs. We demonstrate that convection can dynamically support small scale accumulations of dense ULVZ material, consistent with the size and density inferred from seismology. Furthermore, we show that ULVZs preferentially reside at the boundaries of large compositional reservoirs, which periodically break apart and merge together in response to changes in downwelling patterns. As they do, ULVZ material migrates and recollects in a systematic fashion. ULVZ material can become entrained in mantle plumes forming from reservoir boundaries, contributing to isotopic anomalies found in hotspot volcanism. Thus ULVZ detection helps to constrain large-scale mantle convection patterns, the locations of compositional reservoir boundaries, and the evolution of geochemical reservoirs.

1. Introduction

For over 15 yrs seismologists have mapped regions of ultra-low P- and S-wave velocities at the very base of Earth's mantle at the core-mantle boundary (CMB). Ultra-low velocity zones (ULVZs) have been mapped with thicknesses between 5 and 40 km, with wave speed reductions of 10% and greater. The greatest percentage of the CMB (roughly 40%) has been studied using SPdKS, a wave with short segments of P-wave diffraction at the CMB; but SPdKS has the greatest associated uncertainties unless high resolution waveform modeling is conducted (*e.g*, Rondenay and Fischer, 2003). Using waves that reflect off the CMB (PcP, ScP, ScS) results in imaging ULVZ structure in greater detail, but have a more limited geographical coverage. Fig. 1 and Fig. S1 summarize past work, and show that ULVZs are predominantly found in or near regions where lower mantle shear wave velocity is decreased, in presumed hotter than average lower mantle material.

Some early studies found evidence for the ULVZ S-velocity reduction being up to 3 times that of the P-velocity, and argued for the existence of partial melt as the cause (*e.g,* Rost et al., 2005; Williams and Garnero, 1996). If the lowermost mantle is homogeneous in composition, then a ULVZ caused by partial melt is expected to be nearly global because the CMB is isothermal, and it would have a variable thickness controlled by lowermost mantle temperature. However, many CMB regions lack ULVZ evidence (Fig. 1 and Fig. S1) or do not possess the 3-to-1 S-to-P-wave velocity reduction (e.g, Hutko et al., 2009), which can be reconciled by a chemically distinct component to the ULVZ, whether or not the ULVZ material is partially molten.

One possible source of deep mantle chemical heterogeneity is the seismically-imaged Large Low Shear Velocity Provinces (LLSVPs) at the base of the mantle beneath the Pacific Ocean and Africa (*e.g.,* Dziewonski, 1984; Hernlund and Houser, 2008; Megnin and Romanowicz, 2000; Ritsema et al., 2004; Su and Dziewonski, 1997) (Fig. 1 and Fig. S1). LLSVPs appear to have elevated density (*e.g.,* Ishii and Tromp, 2004; Trampert et al., 2004) and a seismically sharp transition to surrounding mantle (e.g., He and Wen, 2009; Ni et al., 2002; Wang and Wen, 2007). Furthermore, geochemical observations from Earth's surface support the existence of deep mantle

* Corresponding author. Tel.: +1 480 965 1733; fax: +1 480 965 8102.
E-mail address: allen.mcnamara@asu.edu (A.K. McNamara).

0012-821X/$ – see front matter © 2010 Elsevier B.V. All rights reserved.
doi:10.1016/j.epsl.2010.07.042

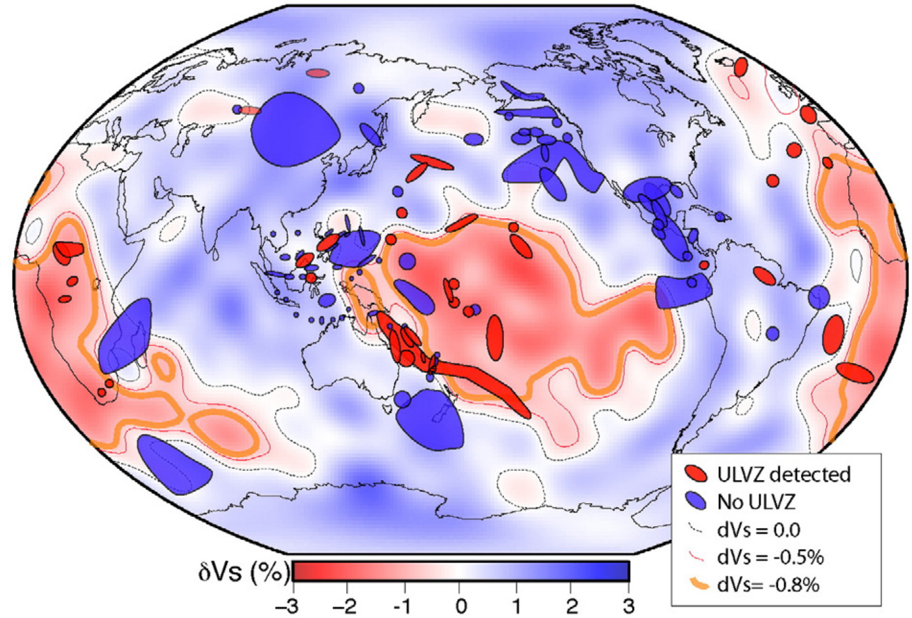

Fig. 1. Global distribution of ULVZ based on seismic studies. Blue areas in the foreground indicate probed areas lacking evidence for ULVZ structure, while red patches in the foreground mark regions with detected ULVZs. Background colors show lowermost mantle seismic shear wave velocities from the tomographic study by Ritsema et al., 2004; scale bar at the bottom is for the background tomography model. Details on studies summarized here can be found in the Supplemental material.

chemical heterogeneity (*e.g.*, Hofmann, 1997). Chemically distinct LLSVPs may have formed by the accumulation of ancient oceanic crust that has long since subducted (*e.g.*, Brandenburg and van Keken, 2007a, 2007b; Brandenburg et al., 2008; Christensen and Hofmann, 1994; Davies, 2008; Hirose et al., 1999; Hofmann and White, 1981; Nakagawa and Buffett, 2005; Nakagawa et al., 2009; Xie and Tackley, 2004a, 2004b), or may be primordial remnants of a mantle differentiation process that occurred much earlier in Earth's history (e.g., Boyet and Carlson, 2005; Kellogg et al., 1999; Labrosse et al., 2007; Lee et al., 2010; Solomatov and Stevenson, 1993; Tolstikhin and Hofmann, 2005). If denser than the background mantle, LLSVP material can survive wholesale entrainment into the convecting mantle, forming long-lived compositional reservoirs (*e.g.*,Bull et al., 2009; Davaille, 1999; Deschamps and Tackley, 2008; 2009; Garnero and McNamara, 2008; Jellinek and Manga, 2002; Kellogg et al., 1999; Lassak et al., 2007, 2010; McNamara and Zhong, 2004a, 2004, 2005; Nakagawa and Tackley, 2008; Olson and Kincaid, 1991; Tackley, 2000, 2002; Tan and Gurnis, 2007, 2005; Youngs and Houseman, 2009; Zhong et al., 2008). This would result in a thermochemical style of mantle convection which is driven by thermal and compositional density variations, with large-scale subduction-driven convection currents that sweep dense basal mantle material towards the upwelling regions beneath the Pacific and Africa, consistent with the location of the LLSVPs (McNamara and Zhong, 2005).

Observed ULVZs (*e.g.*, Idehara et al., 2007; Rost et al., 2005) are at a much smaller length scale (on the order of 10 km thick and 100 km across), which is at least an order of magnitude smaller than the larger LLSVPs imaged beneath the Pacific and Africa (which are of order 100's of km thick, and 1000's of km across). Proposed sources for chemical heterogeneity (*e.g.*, Lay et al., 2004) that might give rise to ULVZs include products associated with mantle-core interaction (*e.g.*, Buffett et al., 2000; Garnero and Jeanloz, 2000; Knittle and Jeanloz, 1991; Mao et al., 2006) and ultra-dense remnants of past subduction (*e.g.*, Dobson and Brodholt, 2005). Like with the much larger, compositionally distinct LLSVPs, it is reasonable to expect that dense ULVZ material would also be swept toward local upwelling regions which should occur along the edges of reservoirs (*e.g.*, Garnero and McNamara, 2008; Hernlund and Tackley, 2007). However, it has not been demonstrated that high density material can accumulate in these regions, and several important questions remain:

1. Can the vigor of deep mantle convection dynamically support topography on material of such high density (as inferred from seismic observations of small scale ULVZs juxtaposed with mantle lacking ULVZ structure), or would high density ULVZ material flatten out into a ubiquitous layer along the CMB?
2. On the other hand, can such small volumes of dense ULVZ material survive intact for geologic times, or would they be completely entrained and mixed with the surrounding mantle?
3. Can changing subduction patterns cause large compositional reservoirs (LLSVPs) to change shape and location over time, and if so, how would accumulations of dense ULVZ material respond to these changes?

To explore these questions, we performed very high resolution, whole mantle, geodynamical convection calculations of a three component thermochemical system: background mantle, large compositional reservoirs intended to represent seismically-observed LLSVPs, and a small volume of very dense ULVZ material. Calculations were performed in two dimensions to achieve a resolution fine enough to capture ULVZ dynamics at the kilometer scale.

Table 1
Cases studied. B_{ULVZ} is the buoyancy ratio of the ULVZ material, and $\Delta\rho/\rho$ is the associated range of density contrasts between ULVZ and background mantle. Typical ULVZ height and width are determined by averaging over multiple time steps and accumulations of ULVZ material. Case 5 is identical to Case 2 except that it employs a compositional dependence of rheology (in addition to temperature-dependent rheology), with ULVZ material being 10 times less viscous.

Case	B_{ULVZ}	$\Delta\rho/\rho$	Typical ULVZ height (km)	Typical ULVZ width (km)	Figure
1	1.0	2.5–5.0%	–	–	2
2	2.0	5.0–10.0%	45	550	3, 4, 5
3	3.0	7.5–15.0%	40	720	S2
4	4.0	10.0–20.0%	30	1150	S3
5	2.0	5.0–10.0%	30	570	5,6

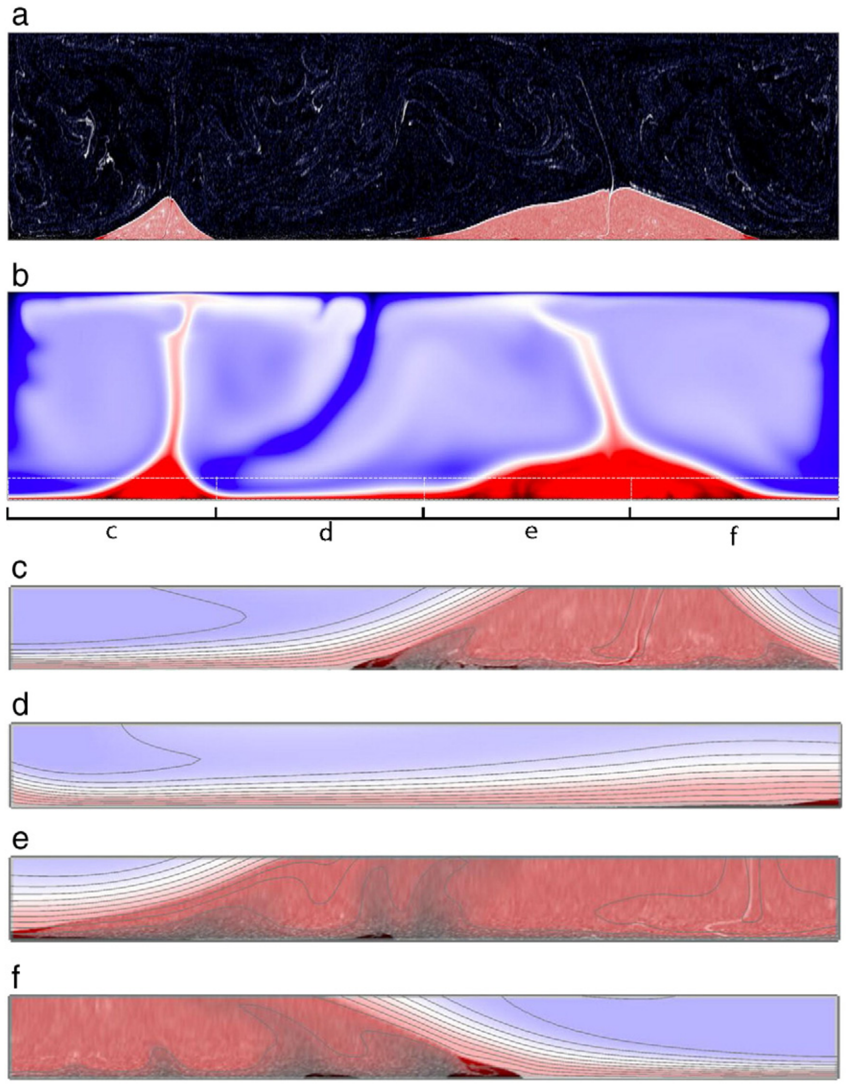

Fig. 2. Composition and temperature of Case 1, shown 250 million years after the start of calculation. a, Compositional field. Background mantle was originally homogeneous (black), and large compositional reservoirs were originally uniform (and solid red). ULVZ material is barely visible on this scale as dark red. White represents a mixture of reservoir material and background mantle. b, Temperature field. Colder and hotter temperatures are represented by darker blue and red colors, respectively. Four boxes at the bottom represent areas that are zoomed-in, shown in panels c–f. c–f, zoom-ins of the boxes shown at the bottom of b, from left to right. Each box is 289 km high. Color represents a superposition of composition and temperature; blue, red, and dark red represent background mantle, compositional reservoirs, and dense ULVZ material respectively. Gray lines are temperature contours, spaced at non-dimensional values of 0.1.

2. Method

The geodynamic calculations are performed by solving the non-dimensional equations for conservation of mass, momentum, and energy using the Boussinesq approximation.

$$\nabla \cdot \vec{u} = 0$$

$$-\nabla P + \nabla \cdot (\eta \dot{\varepsilon}) = Ra(T - BC)\hat{z}$$

$$\frac{\partial T}{\partial t} + (\vec{u} \cdot \nabla)T = \nabla^2 T$$

where u is velocity, P is dynamic pressure, η is viscosity, $\dot{\varepsilon}$ is the strain-rate, T is the temperature, C is composition, $\hat{z}$ is positive in the upward vertical direction, and t is time.

The thermal Rayleigh number is defined as:

$$Ra = \frac{\rho_o g \alpha_o \Delta T h^3}{\eta_o \kappa_o}$$

where ρ_o, α_o, ΔT, η_o, and κ_o are dimensional reference values of density, thermal expansivity, the temperature difference between the core and the surface, upper mantle viscosity at non-dimensional temperature of $T = 0.5$, and thermal diffusivity, respectively. g and h are constants of gravitational acceleration and mantle thickness, respectively. We employ a Rayleigh number of 5×10^7, referenced to upper mantle viscosity at temperature $T = 0.5$. This value of Rayleigh number is consistent with values typically used for mantle convection problems ($\rho_o \sim 3500\ \mathrm{kgm^{-3}}$, $g \sim 10\ \mathrm{ms^{-2}}$, $\alpha_o \sim 10^{-5} K^{-1}$, $\Delta T \sim 3000\ K$, $\eta_o \sim 5 \times 10^{20} Pas$, $\kappa_o \sim 10^{-6} m^2 s$).

Density is represented by the buoyancy ratio, B, defined as:

$$B = \frac{\Delta \rho}{\rho_o \alpha_o \Delta T}$$

where $\Delta \rho$ is the density contrast between particular compositional components. For a given B, one cannot specify a $\Delta\rho/\rho$ with higher certainty than $\alpha\Delta T$. Here we assume that $\alpha\Delta T$ ranges from 0.025–0.05, allowing for uncertainties in α and ΔT. This range of uncertainty was determined by assuming that α is approximately 1.0×10^{-5} to

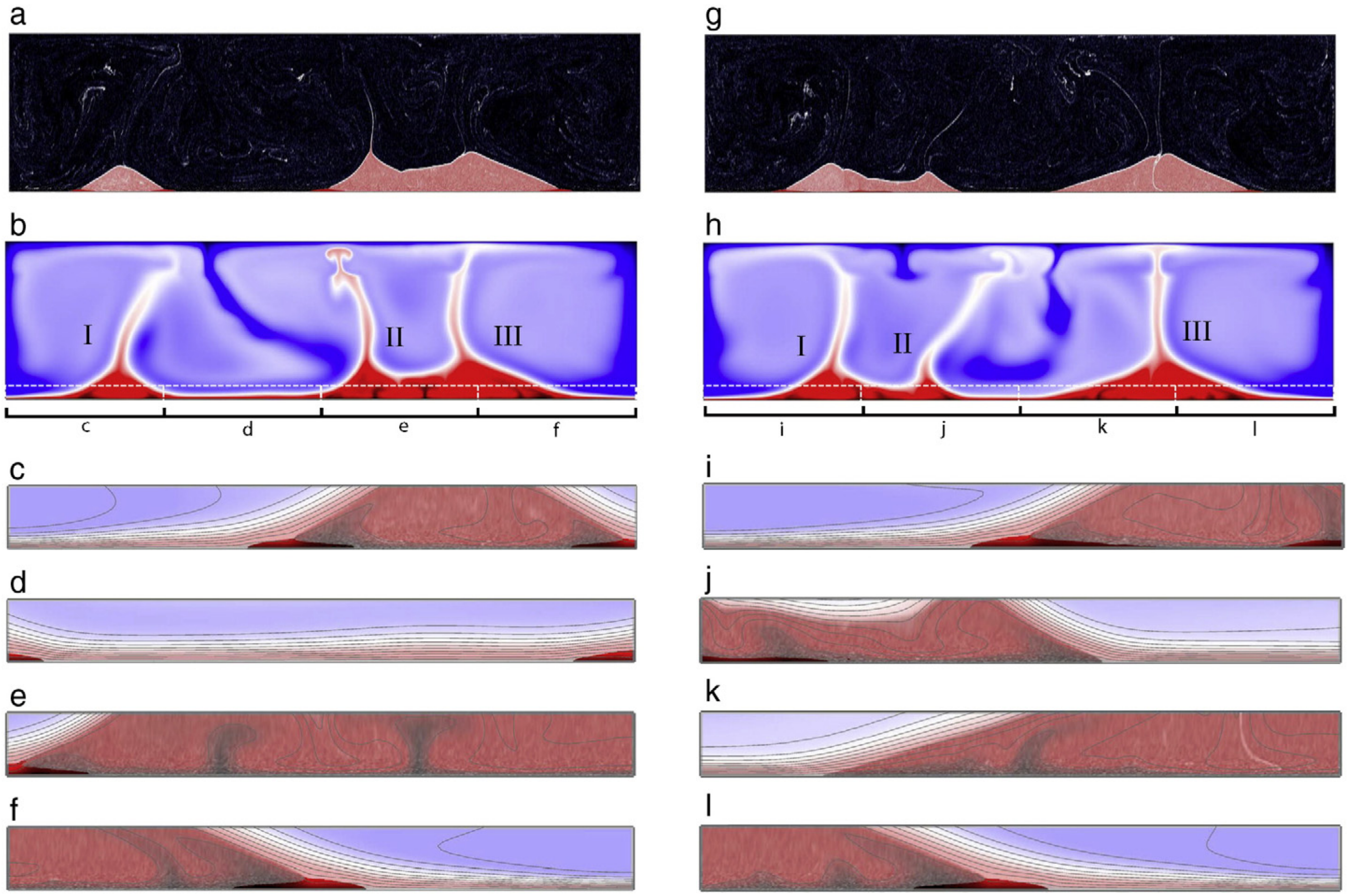

Fig. 3. Composition and temperature of Case 2, shown at two different timesteps. a–f, a snapshot in time (630 million years from start of calculation) before the compositional reservoir on the right breaks apart. Panels represent the same fields and colors as in Fig. 2, except that accumulations of ULVZ are shown here at white. Note that ULVZ material (dark red) accumulates at the base of the boundaries between the large compositional reservoirs and background mantle. g–l, a snapshot at a later time (1.67 billion years from start of calculation), after the compositional reservoir on the right (II + III) breaks apart and a piece of it (II) merges with the reservoir on the left (I). Panels represent the same fields and colors as in Fig. 2. Panels i and j show an orphaned accumulation of ULVZ material temporarily residing at the place where the two compositional reservoirs recently merged. Panels j and k show that the new reservoir boundaries (due to the splitting of a previous, larger reservoir), lack an accumulation of ULVZ material.

$1.5\times10^{-5}\,K^{-1}$ and the potential temperature, ΔT, is approximately 2500-3500 K. Each calculation employed prescribed values of B; therefore, we state density contrast as a range of values in order to reflect this range in $\alpha\Delta T$.

The viscosity η is a function of temperature, depth, and composition, and includes a viscosity increase at the base of the transition zone (equivalently at 660 km depth):

$$\eta(T,z,C) = \eta_z(z)\eta_C(C)\exp[A(0.5-T)]$$

where η_z and z are non-dimensional viscosity and dimensional depth, respectively. $\eta_z(z)=1$ and 50 for the upper and lower mantle, respectively (*e.g.*, Lithgow-Bertelloni and Gurnis, 1997). $\eta_C(C)$is a viscosity coefficient, particular to a given compositional species. For all but Case 5, $\eta_C(C)=1$. A and T are the activation parameter and non-dimensional temperature, respectively. $A=9.2103$, which leads to a viscosity range of 10^4 due to the temperature difference between the hottest and coldest regions of the model.

To solve the conservation equations, we modified the convection code, Citcom (Moresi and Gurnis, 1996) to include thermochemical convection, compositional rheology, and to increase the precision of all variables to double precision (due to the fine grid size in the lowermost part of the model). We used 10 million tracers to track the compositional field using the ratio tracer method (*e.g.*, Tackley and King, 2003).

Temperature boundary conditions are isothermal on the top and bottom and insulating on the sides. Velocity boundary conditions are free-slip on all boundaries. The model domain has an aspect ratio of 4 and the numerical grid incorporates ~0.5 million elements; 1560 in the horizontal direction and 192 in the vertical direction. The grid is gradually refined toward the bottom, providing 2.5 km resolution in the lowermost 40 km of the model. Resolution tests were performed at both higher and lower resolution to ensure that our results are adequately resolved and numerically stable.

The initial condition was established by performing a series of calculations on a 2-component thermochemical system consisting of only background mantle and compositional reservoir material. To aid the system toward reaching a quasi-steady thermal state, we started by using a high buoyancy number for the compositional reservoir material, resulting in a purely layered system. This calculation was performed for many lifetimes of the Earth until it reached equilibrium. Using that layered convection thermal field, we introduced 10 million tracers to represent the compositional reservoirs with a buoyancy number of 0.8 and then performed a series of successive thermochemical calculations, each at higher resolution. At each step of increased resolution, we allowed the models to reach a quasi-steady thermal state. Upon reaching the resolution that was ultimately used for these calculations, we introduced the ULVZ material in the lowermost 5.8 km of the mantle. We investigated several different values of buoyancy number for the

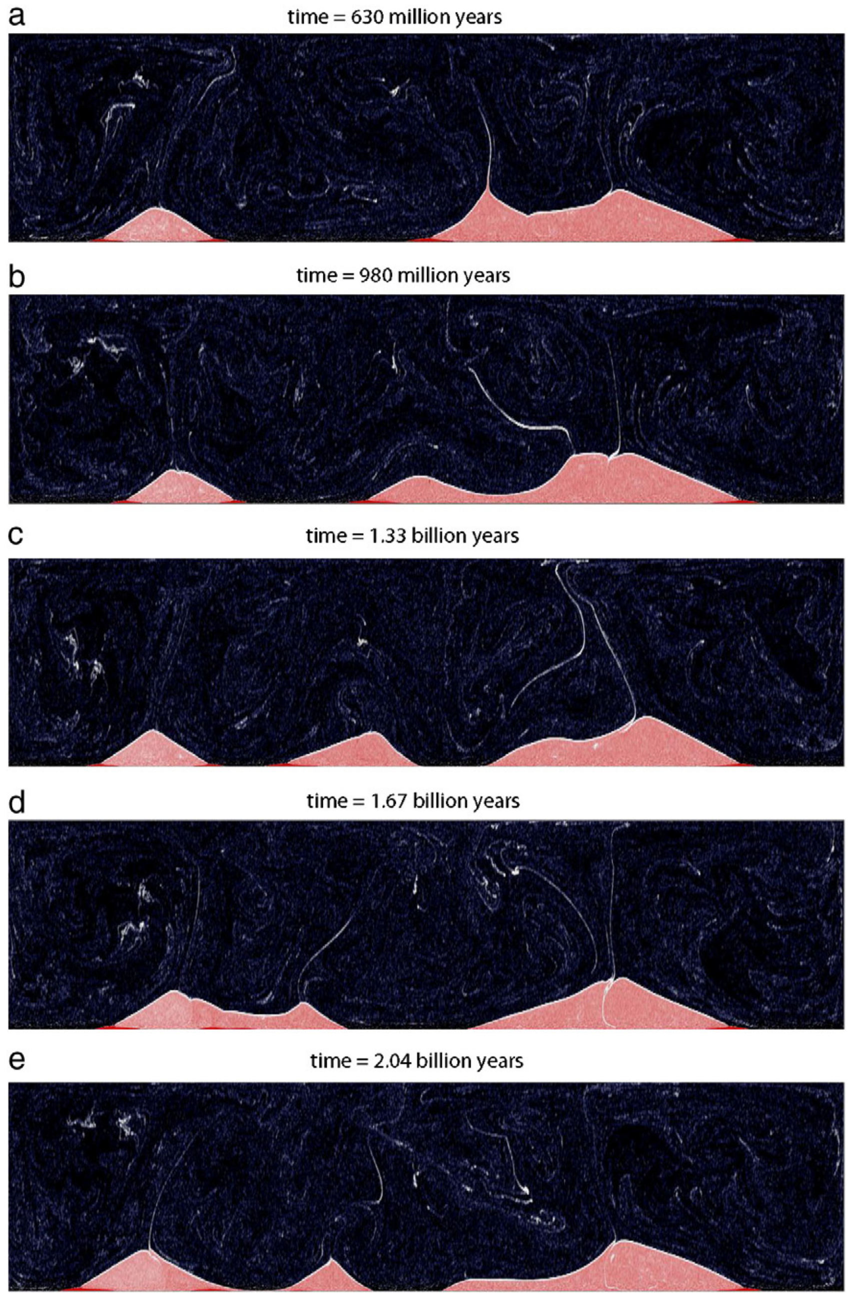

Fig. 4. The time evolution of the compositional field in Case 2. Compositional field at a. 630 million years, b. 980 million years, c. 1.33 billion years, d. 1.67 billion years, and e. 2.04 billion years after the start of the calculation. Black represents background mantle material, light red represents slightly more dense compositional reservoir material, and dark red represents very dense ULVZ material. Regions of white indicate a mixture between background mantle and compositional reservoir material. In a. there are 2 compositional reservoirs, a smaller one on the left and a larger one on the right. In b. the rightmost reservoir begins to break apart. In c. the left part of the original rightmost reservoir has detached and moved toward the reservoir on the left. There are now 3 compositional reservoirs. Note the absence of ULVZ material along the new margins that were created when the reservoir broke apart. In d. the middle reservoir (in c.) has merged with the leftmost reservoir. Note the orphaned accumulation of dense ULVZ material that underlies the merged regions. In e. the reservoir on the left breaks apart; however most of the dense ULVZ material remains in the leftmost reservoir, leaving the middle reservoir with only a very small volume of ULVZ material within it.

compositional reservoirs. $B = 0.8$ was the optimal choice for generating long-lived reservoirs with substantial topography.

The large compositional reservoir (LLSVP) material has a total volume equivalent to a uniform 290 km thick layer at the base of the mantle (10% of the mantle volume) and $B = 0.8$. Dense ULVZ material has a volume equivalent to a uniform 5.8 km thick basal layer (0.2% of the mantle volume), and we vary B from 1.0 to 4.0. For each calculation, we begin with the same starting model, the temperature and compositional field derived from a 2-component calculation (identical to our 3-component system with the dense ULVZ material excluded) that has reached thermal equilibrium. The 5.8 km thick uniform layer of dense ULVZ material is added at the CMB at the initial time and is allowed to evolve. Calculations were carried out for several billion years in model time.

3. Results

Table 1 lists the parameters used in each of our 5 case models. Animations of each case are provided in Supplementary Online Material.

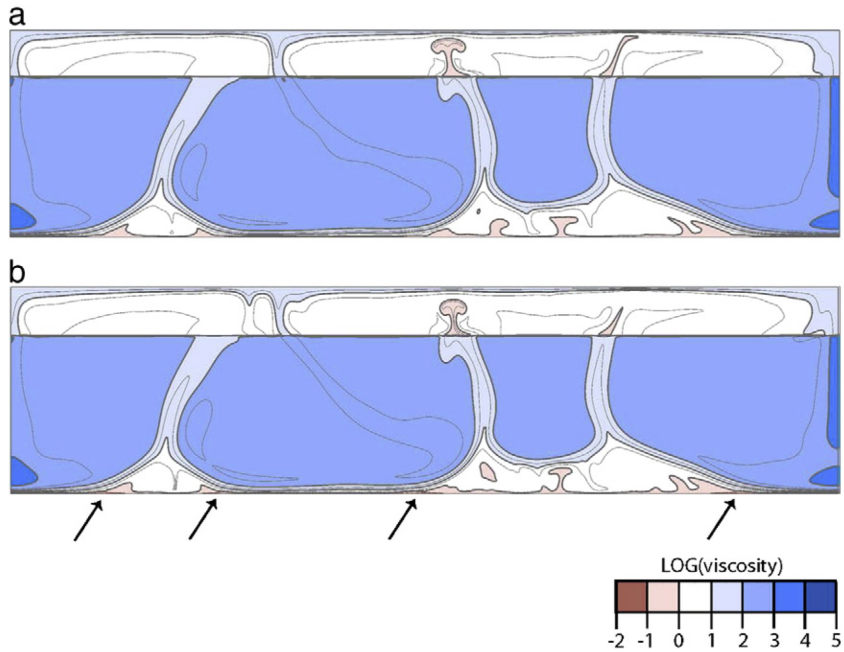

Fig. 5. Viscosity of Case 2 and Case 5. The logarithm of non-dimensional viscosity for a. Case 2 and b. Case 5. Each shade of color represents an order of magnitude value of viscosity (see legend). Contour lines are shown at each half magnitude of viscosity (i.e., every 0.5 in the logarithm of viscosity). Arrows in b. indicate the positions of reduced viscosity due to the accumulation of dense ULVZ material, which are barely visible. Case 2 and Case 5 differ only in Case 5 employing an additional compositional 10× viscosity decrease in the ULVZ material.

Case 1 employs ULVZ material that is 2.5-5% more dense than background mantle ($B=1.0$). Fig. 2a and b show a time snapshot of the temperature and compositional fields, respectively. At this time, two large, lower mantle compositional reservoirs have already formed, shaped by downwellings. Thermal plumes form on the top of the reservoir peaks, entraining and carrying to the surface a small volume of reservoir material. Boxes drawn in the lowermost mantle of Fig. 2b are enlarged and displayed in Fig. 2c-f. The zoomed panels highlight the large compositional reservoirs (light red material), as well as dense ULVZ material present in small regions along the bottom and edges of the reservoirs (dark red). In less than 200 million years, the dense, initially uniform ULVZ layer accumulated at the margins of the compositional reservoirs; however, in this case, ULVZ material was not dense enough to avoid significant entrainment into the compositional reservoir. The accumulation of ULVZ was quickly eroded away and entrained upward along the inside boundary of the reservoir, eventually falling back down to the CMB (Fig. 2c displays a strand of ULVZ material returned to the CMB). ULVZ material then briefly re-accumulates at the reservoir margin before being entrained again. A small degree of ULVZ material escapes the reservoir completely through entrainment into the thermal plumes on top of the reservoir. Ultimately, the ULVZ material completely mixed into the reservoir material, in less than 1 billion years.

Case 2 is identical to Case 1, except that the intrinsic density of the ULVZ material is increased to 5-10% higher than background mantle ($B=2.0$) (Figs. 3 and 4). In this case, the ULVZ was dense enough to avoid entrainment into and mixing with the reservoir. Accumulations of ULVZ material survived until the end of the calculation (4 billion years). Within the first 250 million years, all of the ULVZ material accumulated along the margins of the reservoirs at the CMB, forming stable ULVZ structures that were ~40 km high and ~500 km wide. Fig. 3a-f and g-l represent two different snapshots in time within this Case 2 calculation, separated by 1 billion years of time. Within this time interval, the two reservoirs underwent a dramatic reconfiguration due to a dynamic (not imposed) change in downwelling (Fig. 4). Downwelling occurring in the center-left of the model (Fig. 3b) ceased, and a new downwelling formed off to the right (Fig. 3h). In response, the rightmost reservoir (combined II and III, Fig. 3b) separated into two, smaller reservoirs (separated II and III, Fig. 3h); the leftmost of which (II, Fig. 3h) was swept toward the left and merged with the other reservoir (I, Fig. 3h). Upon merging, the ULVZ material that had previously resided at the reservoirs' leading edges also merged, resulting in an orphaned accumulation of ULVZ material along the CMB in the middle of the new, combined reservoir (Fig. 3h (I + II), 3i-j). This orphaned accumulation of ULVZ became unstable and flattened out along the reservoir bottom, gradually re-accumulating at the new reservoir (I + II) boundaries in about 500 million years. After the bifurcation of reservoirs II + III into I + II, the leftover remnant of the rightmost reservoir III has not yet reacquired an accumulation of ULVZ material at its newly-formed leftmost boundary (Fig. 3k).

We examined other cases with higher ULVZ densities, (Cases 3-4, Table 1, Figs. S2 and S3) and we found that as ULVZ density is increased, ULVZs become thinner and wider (Table 1). Aside from being more flattened out, ULVZ material followed the same dynamic trends as observed in Case 2; ULVZ material quickly accumulated along reservoir edges until temporarily disrupted by a reorganization of the larger compositional reservoirs.

Cases 1-4 employed the same rheological formulation for all three chemically distinct components of the mantle system. Temperature dependence of viscosity led to large viscosity contrasts between ULVZ, reservoirs, and background mantle material (Fig. 5a). Because reservoir margins are the hottest regions in the mantle, ULVZ material in those locations had a viscosity that was an order of magnitude smaller than that of the reservoirs and two to three orders of magnitude smaller than background mantle. This explains the asymmetrical shape of the ULVZ accumulations as a result of differential viscous coupling (e.g., Fig. 3c, f, i, and l); the side of the ULVZ fully in the reservoir is thinner than the side in contact with the cooler background mantle. If some ULVZs contain partial melt, viscosity could be further reduced (*e.g.,* Hier-Majumder, 2008). Case 5 is identical to Case 2 except that the viscosity of the ULVZ material was reduced by an order of magnitude, in addition to the reduction due to temperature dependence (i.e., $\eta_C(C)=0.1$ for the ULVZ material) (Fig. 5b). The resultant ULVZ accumulations exhibited a slightly more flattened topography than Case 2 (Table 1, Fig. 6).

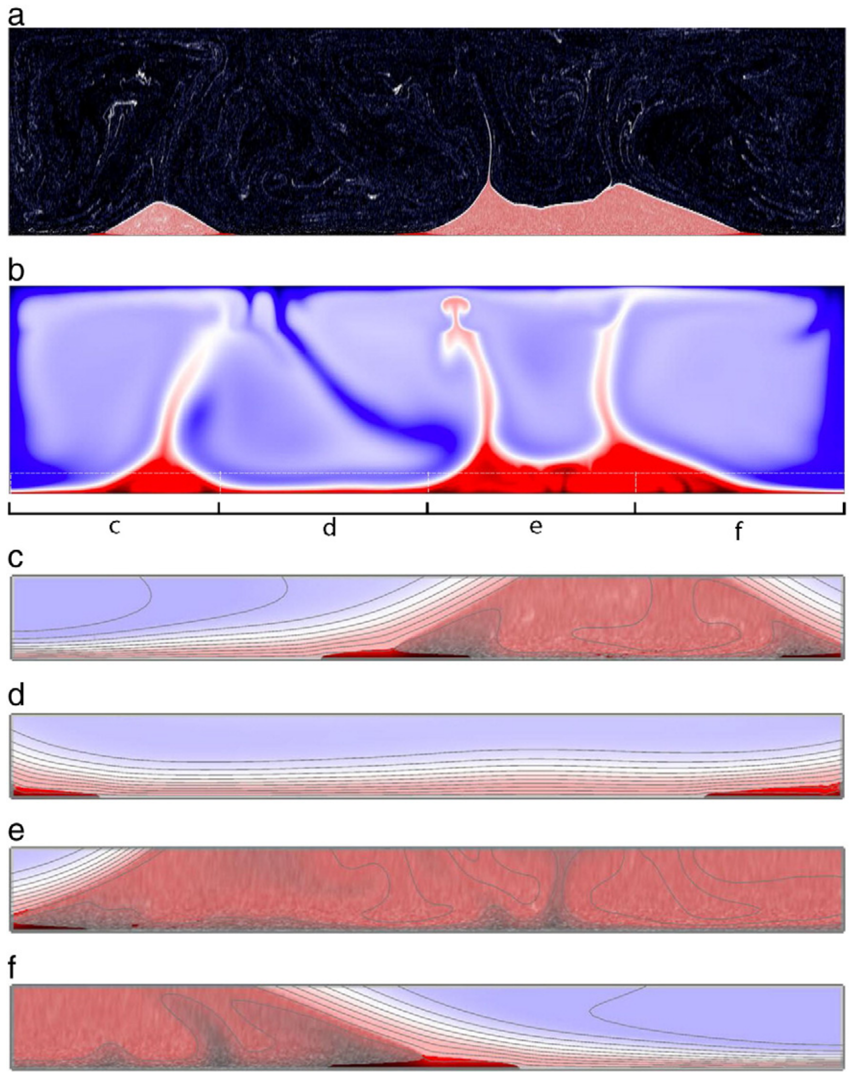

Fig. 6. Composition and temperature of Case 5, shown 630 million years after the start of calculation. This case is identical to Case 2 except that ULVZ material has an additional 10× viscosity decrease due to composition. a, Compositional field. Background mantle was originally homogeneous (black), and large compositional reservoirs were originally uniform (and solid red). ULVZ material is barely visible on this scale as dark red. White represents a mixture of reservoir material and background mantle. b, Temperature field. Colder and hotter temperatures are represented by darker blue and red, respectively. Four boxes at the bottom represent areas that are zoomed-in, shown in panels c–f. c–f, zoom-ins of the boxes shown at the bottom of b, from left to right. Each box is 289 km high. Color represents a superposition of composition and temperature; blue, red, and dark red represent background mantle, compositional reservoirs, and dense ULVZ material respectively. Gray lines are temperature contours, spaced at non-dimensional values of 0.1. The 10× viscosity decrease in ULVZ material has caused the accumulations of dense ULVZ to be slightly thinner and wider than those in Case 2.

3.1. Discussion and Conclusions

This work assumes a compositional origin to ULVZs which is motivated by seismic studies that infer the presence of isolated ULVZ patches surrounded by non-ULVZ (e.g., Idehara et al., 2007; Rost et al., 2005), and ULVZ regions that do not exhibit a 3-to-1 δV_s-to-δV_p velocity reduction (*e.g.,* Castle and van der Hilst, 2000; Hutko et al., 2009; Thorne and Garnero, 2004). If ULVZs are compositional anomalies, it is plausible that they contain some partial melt because they are located in the hottest CMB regions. This work presumes that the presence of partial melt does not feed back into the dynamics other than as a viscosity reduction (i.e. Case 5). For high degrees of partial melting (and hence a greater viscosity reduction), especially in the presence of strong lateral variability in melt concentration, it is unclear how the dynamics would be affected, particularly if melt is able to percolate downward faster than its matrix is being advected upward, possibly forming a thin melt layer along the CMB (*e.g.,* Hernlund and Tackley, 2007; Rost et al., 2005). However, some models indicate that viscous stresses may be able to drive melt against gravity (Hernlund and Jellinek, 2010). ULVZs may contain elements apparently missing from mid-ocean ridge basalts that are observed in ocean island basalts, since plumes preferentially form from the chemical reservoir boundaries which can entrain ULVZ material (*e.g.,* Hofmann, 1997).

In the calculations provided here, we have kept all parameters fixed while varying the density of ULVZ material. Surely, the numerical values of $\Delta\rho/\rho$, ULVZ height, and ULVZ width provided in Table 1 are related to the parameters that we have held fixed (i.e., the Rayleigh number, temperature dependence of rheology, viscosity increase between upper and lower mantle, etc.). Therefore, these numerical values are useful in a comparative context, and one must use caution not to consider them as being constrained by the modeling. Furthermore, we have assumed incompressibility, constant thermal expansivity, and constant thermal diffusivity in these calculations. . Future work will explore the sensitivity of ULVZ morphology and minimum density to the parameters held fixed in this study.

Our modeling directly links the locations of LLSVP margins and ULVZs. The resolution of seismic tomography is not high enough to image sharp, compositional reservoir boundaries; seismic waveform analyses are necessary (e.g., Ni et al., 2002; He and Wen, 2009; Wang and Wen, 2007). Thus mapping out the geographical distribution of ULVZs provides an additional, complementary tool toward identifying lowermost mantle compositional reservoir boundaries. Our calculations also indicate they contain information about the time evolution and dynamics of the large reservoirs. Isolated ULVZs located within the central region of large LLSVPs (Fig. 1) may mark internal boundaries (i.e., the presence of multiple thermochemical structures, which are collectively mapped by tomography as a single LLSVP), or they may be temporary, orphaned ULVZ remnants leftover from a geologically recent merger of two reservoirs. The former has been inferred from recent seismic studies (He and Wen, 2009) and the latter has been observed in geodynamical models that employ plate motions as surface boundary conditions (McNamara and Zhong, 2005).

In conclusion, we find that ULVZ material with an intrinsic density increase similar to that inferred from seismic studies can be dynamically supported along the boundaries of compositional reservoirs into structures having a morphology consistent with constraints from array analyses of core-reflected phases (*e.g.*, Idehara et al., 2007; Rost et al., 2005). For the calculations performed here, we find that ULVZ material must exceed a minimum density increase of 5% higher than the background mantle to survive entrainment and mixing into the surrounding mantle. We also find that temporally changing downwelling patterns are expected to lead to major reconfigurations of the large compositional reservoirs, and ULVZ material adjusts to new reservoir boundaries on a characteristic timescale of 250-500 million years. These calculations predict that ULVZs may not be present at all reservoir boundaries, particularly after a major reservoir reconfiguration; however, ULVZs should predominantly exist at reservoir boundaries. Observed ULVZ and implied LLSVP locations (Fig. 1) are consistent with a chemical heterogeneity origin of ULVZs and are difficult to explain by partial melt alone. Our calculations predict that ULVZs accumulating along reservoir boundaries should be thicker on one side of the ULVZ due to differing magnitudes of viscous coupling with the hotter reservoir versus the cooler background mantle. This may be seismically testable, and would further confirm the existence of long-clived compositional reservoirs in Earth's lower mantle.

Supplementary materials related to this article can be found online at doi:10.1016/j.epsl.2010.07.042.

Acknowledgements

We thank Paul Tackley and an anonymous reviewer for constructive comments. This work was supported by NSF grants EAR-0510383 and EAR-0456356 (A.K.M) and by NSF grants EAR-0711401 and EAR-0453944 (E.J.G).

References

Brandenburg, J.P., van Keken, P.E., 2007a. Deep storage of oceanic crust in a vigorously convecting mantle. Journal of Geophysical Research, Solid Earth 112 (B6). doi:10.1029/2006jb004813.

Brandenburg, J.P., van Keken, P.E., 2007b. Methods for thermochemical convection in earth's mantle with force-balanced plates. Geochemistry, Geophysics, Geosystems 8. doi:10.1029/2007gc001692.

Brandenburg, J.P., Hauri, E.H., van Keken, P.E., Ballentine, C.J., 2008. A multiple-system study of the geochemical evolution of the mantle with force-balanced plates and thermochemical effects. Earth and Planetary Science Letters 276 (1–2), 1–13.

Boyet, M., Carlson, R.W., 2005. ^{142}Nd evidence for early (>4.53 Ga) global differentiation of the silicate earth. Science 309 (576), 576–581.

Buffett, B.A., Garnero, E.J., Jeanloz, R., 2000. Sediments at the top of Earth's core. Science 290 (5495), 1338–1342.

Bull, A.L., McNamara, A.K., Ritsema, J., 2009. Synthetic tomography of plume clusters and thermochemical piles. Earth and Planetary Science Letters 278 (3–4), 152–162.

Castle, J.C., van der Hilst, R.D., 2000. The core–mantle boundary under the Gulf of Alaska: NoULVZ for shear waves. Earth and Planetary Science Letters 176 (3–4), 311–321.

Christensen, U.R., Hofmann, A.W., 1994. Segregation of subducted oceanic-crust in the convecting mantle. Journal of Geophysical Research, Solid Earth 99 (B10), 19867–19884.

Davaille, A., 1999. Simultaneous generation of hotspots and superswells by convection in a heterogenous planetary mantle. Nature 402 (6763), 756–760.

Davies, G.F., 2008. Episodic layering of the early mantle by the 'basalt barrier' mechanism. Earth and Planetary Science Letters 275 (3–4), 382–392.

Deschamps, F., Tackley, P.J., 2008. Searching for models of thermo-chemical convection that explain probabilistic tomography I, principles and influence of rheological parameters. Physics of the Earth and Planetary Interiors 171 (1–4), 357–373.

Deschamps, F., Tackley, P.J., 2009. Searching for models of thermo-chemical convection that explain probabilistic tomography, II-influence of physical and compositional parameters. Physics of the Earth and Planetary Interiors 176 (1–2), 1–18.

Dobson, D.P., Brodholt, J.P., 2005. Subducted banded iron formations as a source of ultralow-velocity zones at the core–mantle boundary. Nature 434 (7031), 371–374.

Dziewonski, A.M., 1984. Mapping the lower mantle — determination of lateral heterogeneity in P-velocity up to degree and order-6. Journal of Geophysical Research 89 (Nb7), 5929–5952.

Garnero, E.J., Jeanloz, R., 2000. Fuzzy patches on the Earth's core–mantle boundary? Geophysical Research Letters 27 (17), 2777–2780.

Garnero, E.J., McNamara, A.K., 2008. Structure and dynamics of Earth's lower mantle. Science 320 (5876), 626–628.

He, Y.M., Wen, L.X., 2009. Structural features and shear-velocity structure of the "Pacific Anomaly". Journal of Geophysical Research, Solid Earth 114. doi:10.1029/2008jb005814.

Hernlund, J.W., Tackley, P.J., 2007. Some dynamical consequences of partial melting in Earth's deep mantle. Physics of the Earth and Planetary Interiors 162 (1–2), 149–163.

Hernlund, J.W., Houser, C., 2008. The statistical distribution of seismic velocities in Earth's deep mantle. Earth and Planetary Science Letters 265 (3–4), 423–437.

Hernlund, J.W., Jellinek, A.M., 2010. Dynamics and structure of a stirred partially molten ultralow velocity zone. Earth and Planetary Science Letter 296, 1–8.

Hier-Majumder, S., 2008. Influence of contiguity on seismic velocities of partially molten aggregates. Journal of Geophysical Research, Solid Earth 113 (B12). doi:10.1029/2008jb005662.

Hirose, K., Fei, Y.W., Ma, Y.Z., Mao, H.K., 1999. The fate of subducted basaltic crust in the Earth's lower mantle. Nature 397 (6714), 53–56.

Hofmann, A.W., 1997. Mantle geochemistry: the message from oceanic volcanism. Nature 385 (6613), 219–229.

Hofmann, A.W., White, W.M., 1981. Mantle plumes from ancient oceanic crust. Earth and Planetary Science Letters 57, 421–436.

Hutko, A.R., Lay, T., Revenaugh, J., 2009. Localized double-array stacking analysis of PcP: D'' and ULVZ structure beneath the Cocos plate, Mexico, central Pacific, and north Pacific. Physics of the Earth and Planetary Interiors 173 (1–2), 60–74.

Idehara, K., Yamada, A., Zhao, D., 2007. Seismological constraints on the ultralow velocity zones in the lowermost mantle from core-reflected waves. Physics of the Earth and Planetary Interiors 165 (1–2), 25–46.

Ishii, M., Tromp, J., 2004. Constraining large-scale mantle heterogeneity using mantle and inner-core sensitive normal modes. Physics of the Earth and Planetary Interiors 146 (1–2), 113–124.

Jellinek, A.M., Manga, M., 2002. The influence of a chemical boundary layer on the fixity, spacing and lifetime of mantle plumes. Nature 418 (6899), 760–763.

Kellogg, L.H., Hager, B.H., van der Hilst, R.D., 1999. Compositional stratification in the deep mantle. Science 283 (5409), 1881–1884.

Knittle, E., Jeanloz, R., 1991. Earth's core–mantle boundary — results of experiments at high-pressures and temperatures. Science 251 (5000), 1438–1443.

Labrosse, S., Hernlund, J.W., Coltice, N., 2007. A crystallizing dense magma ocean at the base of the Earth's mantle. Nature 450 (7171), 866–869.

Lassak, T.M., McNamara, A.K., Zhong, S., 2007. Influence of thermochemical piles on topography at Earth's core–mantle boundary. Earth and Planetary Science Letters 261 (3–4), 443–455.

Lassak, T.M., McNamara, A.K., Garnero, E.J., Zhong, S.J., 2010. Core–mantle boundary topography as a possible constraint on lower mantle chemistry and dynamics. Earth and Planetary Science Letters 289 (1–2), 232–241.

Lay, T., Garnero, E.J., Williams, Q., 2004. Partial melting in a thermo-chemical boundary layer at the base of the mantle. Physics of the Earth and Planetary Interiors 146 (3–4), 441–467.

Lee, C.T.A., Luffi, P., Hoink, T., Li, J., Dasgupta, R., Hernlund, J., 2010. Upside-down differentiation and generation of a 'primordial' lower mantle. Nature 463 (7283), 930-U102.

Lithgow-Bertelloni, C., Gurnis, M., 1997. Cenozoic subsidence and uplift of continents from time-varying dynamic topography. Geology 25, 735–738.

Mao, W.L., Mao, H.K., Sturhahn, W., Zhao, J.Y., Prakapenka, V.B., Meng, Y., Shu, J.F., Fei, Y.W., Hemley, R.J., 2006. Iron-rich post-perovskite and the origin of ultralow-velocity zones. Science 312 (5773), 564–565.

McNamara, A.K., Zhong, S.J., 2004a. Thermochemical structures within a spherical mantle: superplumes or piles? Journal of Geophysical Research, Solid Earth 109 (B7). doi:10.1029/2003jb002847.

McNamara, A.K., Zhong, S.J., 2004b. The influence of thermochemical convection on the fixity of mantle plumes. Earth and Planetary Science Letters 222 (2), 485–500.

McNamara, A.K., Zhong, S.J., 2005. Thermochemical structures beneath Africa and the Pacific Ocean. Nature 437 (7062), 1136–1139.

Megnin, C., Romanowicz, B., 2000. The three-dimensional shear velocity structure of the mantle from the inversion of body, surface and higher-mode waveforms. Geophysical Journal International 143 (3), 709–728.

Moresi, L., Gurnis, M., 1996. Constraints on the lateral strength of slabs from three-dimensional dynamic flow models. Earth and Planetary Science Letters 138 (1–4), 15–28.

Nakagawa, T., Buffett, B.A., 2005. Mass transport mechanism between the upper and lower mantle in numerical simulations of thermochemical mantle convection with multicomponent phase changes. Earth and Planetary Science Letters 230, 11–27.

Nakagawa, T., Tackley, P.J., 2008. Lateral variations in CMB heat flux and deep mantle seismic velocity caused by a thermal–chemical–phase boundary layer in 3D spherical convection. Earth and Planetary Science Letters 271 (1–4), 348–358.

Nakagawa, T., Tackley, P.J., Deschamps, F., Connolly, J.A.D., 2009. Incorporating self-consistently calculated mineral physics into thermochemical mantle convection simulations in a 3-D spherical shell and its influence on seismic anomalies in Earth's mantle. Geochemistry, Geophysics, Geosystems 10. doi:10.1029/2008GC002280.

Ni, S.D., Tan, E., Gurnis, M., Helmberger, D., 2002. Sharp sides to the African superplume. Science 296 (5574), 1850–1852.

Olson, P., Kincaid, C., 1991. Experiments on the interaction of thermal-convection and compositional layering at the base of the mantle. Journal of Geophysical Research-Solid Earth and Planets 96 (B3), 4347–4354.

Ritsema, J., van Heijst, H.J., Woodhouse, J.H., 2004. Global transition zone tomography. Journal of Geophysical Research, Solid Earth 109 (B2). doi:10.1029/2003jb002610.

Rondenay, S., Fischer, K.M., 2003. Constraints on localized core–mantle boundary structure from multichannel, broadband SKS coda analysis. Journal of Geophysical Research, Solid Earth 108 (B11). doi:10.1029/2003jb002518.

Rost, S., Garnero, E.J., Williams, Q., Manga, M., 2005. Seismological constraints on a possible plume root at the core–mantle boundary. Nature 435 (7042), 666–669.

Solomatov, V.S., Stevenson, D.J., 1993. Suspension in convective layers and style of differentiation of a terrestrial magma ocean. Journal of Geophysical Research 98 (E3), 5375–5390.

Su, W.J., Dziewonski, A.M., 1997. Simultaneous inversion for 3-D variations in shear and bulk velocity in the mantle. Physics of the Earth and Planetary Interiors 100 (1–4), 135–156.

Tackley, P.J., 2000. Mantle convection and plate tectonics: toward an integrated physical and chemical theory. Science 288 (5473), 2002–2007.

Tackley, P.J., 2002. Strong heterogeneity caused by deep mantle layering. Geochemistry, Geophysics, Geosystems 3. doi:10.1029/2001gc000167.

Tackley, P.J., King, S.D., 2003. Testing the tracer ratio method for modeling active compositional fields in mantle convection simulations. Geochemistry, Geophysics, Geosystems 4. doi:10.1029/2001gc000214.

Tan, E., Gurnis, M., 2005. Metastable superplumes and mantle compressibility. Geophysical Research Letters 32 (20). doi:10.1029/2005gl024190.

Tan, E., Gurnis, M., 2007. Compressible thermochemical convection and application to lower mantle structures. Journal of Geophysical Research, Solid Earth 112 (B6). doi:10.1029/2006jb004505.

Thorne, M.S., Garnero, E.J., 2004. Inferences on ultralow-velocity zone structure from a global analysis of SPdKS waves. Journal of Geophysical Research, Solid Earth 109 (B8). doi:10.1029/2004jb003010.

Tolstikhin, I., Hofmann, A.W., 2005. Early crust on top of the Earth's core. Physics of the Earth and Planetary Interiors 148, 109–130.

Trampert, J., Deschamps, F., Resovsky, J., Yuen, D., 2004. Probabilistic tomography maps chemical heterogeneities throughout the lower mantle. Science 306 (5697), 853–856.

Wang, Y., Wen, L.X., 2007. Geometry and P and S velocity structure of the "African Anomaly". Journal of Geophysical Research, Solid Earth 112 (B5). doi:10.1029/2006jb004483.

Williams, Q., Garnero, E.J., 1996. Seismic evidence for partial melt at the base of Earth's mantle. Science 273 (5281), 1528–1530.

Xie, S., Tackley, P.J., 2004a. Evolution of U–Pb and Sm–Nd systems in numerical models of mantle convection and plate tectonics. Journal of Geopysical Research 109, B11204. doi:10.1029/2004JB003176.

Xie, S., Tackley, P.J., 2004b. Evolution of helium and argon isotopes in a convecting mantle. Physics of the Earth and Planetary Interiors 146, 417–439.

Youngs, B.A.R., Houseman, G.A., 2009. Formation of steep-sided topography from compositionally distinct dense material at the base of the mantle. Journal of Geophysical Research, Solid Earth 114. doi:10.1029/2007jb005487.

Zhong, S.J., McNamara, A., Tan, E., Moresi, L., Gurnis, M., 2008. A benchmark study on mantle convection in a 3-D spherical shell using CitcomS. Geochemistry, Geophysics, Geosystems 9. doi:10.1029/2008gc002048.